

Tao SUN, Lufang QIN, Junming HOU, Yucan FU

Machinability of damage-tolerant titanium alloy in orthogonal turn-milling

© Higher Education Press 2020

Abstract The damage-tolerant titanium alloy TC21 is used extensively in important parts of advanced aircraft because of its high strength and durability. However, cutting TC21 entails problems, such as high cutting temperature, high tool tip stress, rapid tool wear, and difficulty guaranteeing processing quality. Orthogonal turn-milling can be used to solve these problems. In this study, the machinability of TC21 in orthogonal turn-milling is investigated experimentally to optimize the cutting parameters of orthogonal turn-milling and improve the machining efficiency, tool life, and machining quality of TC21. The mechanism of the effect of turn-milling parameters on tool life is discussed, the relationship between each parameter and tool life is analyzed, and the failure process of a TiAlN-coated tool in turn-milling is explored. Experiments are conducted on the integrity of the machined surface (surface roughness, metallographic structure, and work hardening) by turn-milling, and how the parameters influence such integrity is analyzed. Then, reasonable cutting parameters for TC21 in orthogonal turn-milling are recommended. This study provides strong guidance for exploring the machinability of difficult-to-cut materials in orthogonal turn-milling and improves the applicability of orthogonal turn-milling for such materials.

Keywords orthogonal turn-milling, damage-tolerant titanium alloy, tool life and failure, machined surface integrity, machinability

Received October 11, 2019; accepted January 6, 2020

Tao SUN (✉), Lufang QIN

Jiangsu Key Laboratory of Large Engineering Equipment Detection and Control, Xuzhou University of Technology, Xuzhou 221111, China
E-mail: suntao@xzit.edu.cn

Junming HOU

Industrial Center, Nanjing Institute of Technology, Nanjing 211167, China

Yucan FU

College of Mechanical and Electrical Engineering, Nanjing University of Aeronautics and Astronautics, Nanjing 210016, China

1 Introduction

As a damage-tolerant titanium alloy, TC21 has better mechanical and technical properties than medium-strength titanium alloys TC4 and TA15; TC21 has high strength, high toughness, high damage tolerance, good fatigue performance, simple heat-treatment process, good forgeability, and excellent welding performance [1–3]. Thus, TC21 is used extensively in the important parts of advanced aircraft that require high strength and durability, such as the middle and back fuselage, wings, and undercarriage.

However, the machinability of TC21 must be improved before this alloy can be used widely in other aerospace applications, but only a few studies have been conducted on the machinability of TC21 thus far. Using the same tool and cutting parameters, Shi et al. [4,5] experimentally showed that the tool life of milling TC21 is around a third of that of milling TC4. Sun et al. [1,6] studied the machinability of turning and plunge-milling TC21; they found that its machinability is inferior to that of TC4 and recommended suitable machining parameters. Zhang et al. [7] experimentally studied the cutting force and tool wear of dry high-speed milling. Their results showed that the cutting force in milling TC21 is much higher than that in milling TC4. They concluded that TC21 is harder to mill than TC4, and the main tool wear mode of a TiAlN–TiN-coated carbide tool is crater wear at the flank.

Between TC4 and TC21, the latter has higher strength, hardness, and impact toughness and lower thermal conductivity and contraction of the cross-sectional area. This combination of physical characteristics and the basket-weave microstructure of TC21 make the cutting force and cutting temperature of TC21 higher than that of TC4 and its cutting machinability worse than that of TC4 [6,8]. The cutting of TC21 is affected by high cutting temperature, high tool tip stress, rapid tool wear, and low processing quality.

For rotating parts with typical mechanical structures (e.g., slender rods and undercarriage), the poor cutting

machinability of TC21 and the weak rigidity of structures cause problems during cutting, such as easy machining deformation, reduced tool life, low processing quality, and low machining efficiency. These restrict the aerospace applications of TC21. The following approaches can be used to make TC21 easy to cut: Optimized tool construction, use of advanced tool materials, improved design of the cooling medium and cooling equipment, unconventional cutting technology, and appropriate heat treatment. Several of these approaches require re-developed tools and extra equipment, and others are difficult to control. In addition, the improved machinability of TC21 is unstable when certain methods are utilized, thereby making these methods difficult to implement in factories.

Through the combination of a slowly rotating workpiece and fast-rotating, straight-line motion of the milling cutter, turn-milling can realize high-efficiency machining, which offers improved machined surface integrity, prolonged tool life, and increased machining efficiency to many materials. Schulz and Spur [9] and Schulz and Kneisel [10] were the first to propose turn-milling. They investigated the use of the carbide tool P20/30, CBN, and a composite ceramic coating to cut bearing steel 100Cr6 ($HRC \geq 62$) by turn-milling, and they measured tool wear, the machined surface roughness, and the surface morphology of the workpiece. Their study showed that turn-milling offers high-speed machining to a slowly rotating workpiece. The machined surface roughness, R_a , of the workpiece is less than that obtained in turning and even equal to that obtained in grinding. The results of Ref. [9,10] offer a new method of cutting that is particularly suitable for parts that require grinding after turning and provide guidance for the turn-milling of difficult-to-cut materials and large thin-wall rotary parts.

Choudhury and Mangrulkar [11] and Choudhury and Bajpai [12] experimentally analyzed the machined surface roughness (R_a) of turn-milling in mild steel and brass workpieces by using a high-speed steel milling cutter. The results showed that the chips produced in turn-milling are fewer than those produced in turning, so the value of R_a achieved by turn-milling is around one-tenth of that achieved by turning. With the same material removal rate (MRR) and feed, Ekinović et al. [13] experimentally confirmed that turn-milling is particularly suitable for processing normalized steel, ductile steel, and brass and that the roughness values (R_a , R_z , and R_{max}) of turn-milling are far smaller than those of turning. Pogacnik and Kopac [14] optimized entry and exit conditions and avoided the dynamic instability of turn-milling by using simulations and tool wear measurements; compared with turning, turn-milling offers easier high-speed cutting and lower surface roughness at the same productivity. Zhu et al. [15] used simulations and experiments to discuss the effects of cutting parameters in turn-milling; their results showed that using optimum cutting parameters results in high surface quality with a tiny oil storage structure. Ratnam et al. [16]

studied machined surface roughness and hardness by measuring the signal-to-noise ratio of the responses and analyzing the variance; they showed that feed rate and tool speed are highly significant for R_a and that cutting depth and tool speed are important for surface hardness. Karagüzel et al. [17–20] analyzed the cutting forces and cutting heat in turn-milling and optimized the processes. They machined three difficult-to-cut-materials (Waspaloy, Ti6Al4V, and Inconel 718) under dry, flood-coolant, and minimum-quantity lubrication conditions. They showed that turn-milling has the advantages of low temperature and long tool life, thus making turn-milling suitable for cutting difficult-to-cut-materials that have low thermal conductivity. Niu et al. [21] used a box-counting method to evaluate the surface quality of miniature parts machined by turn-milling. The results indicated that low workpiece speed, low feed rate per revolution, and proper cutting depth result in improved surface quality. Berenji et al. [22] considered the machined surface quality, cutting time, and cost via turning and turn-milling experiments using two difficult-to-cut-materials (AISI 316 stainless steel and Waspaloy). Compared with turning, turn-milling offers better machined surface quality, tool life, and machining productivity. Benjamin et al. [23] investigated the surface integrity of turn-milling in terms of roughness, imperfections, and compressive residual stress and found that reasonable cutting parameters and tool clearance angle can reduce the formation of surface imperfections.

These studies have shown that turn-milling demonstrates advantages over turning when the aim is to machine difficult-to-cut-materials. First, the interrupted cutting process of turn-milling helps reduce the cutting temperature. Second, the small chip volume leads to low cutting forces. Third, even with slow chuck rotation, turn-milling offers easy high-speed cutting by using a high tool rotation speed. These three reasons show that turn-milling has higher cutting efficiency, better machined surface quality, and longer tool life compared with turning in same material removal, thereby making turn-milling suitable for machining difficult-to-cut-materials (e.g., stainless steel, Ti alloys, and nickel alloys) and special rotary parts (e.g., slender rods, thin-wall rotary parts, crankshafts, and turbine blades) [24].

On the basis of the relative positions of the workpiece and tool, turn-milling can be classified as (i) orthogonal, (ii) axial, and (iii) tangential. Orthogonal turn-milling is the most popular type because of the restricted tool length or workpiece diameter. To cut TC21 via orthogonal turn-milling, machinability, which involves tool life, machining efficiency, and machined surface integrity, must be investigated comprehensively. We therefore examine how orthogonal turn-milling parameters affect tool life, and we analyze the tool failure process and mechanism. We also study the machined surface integrity, including surface roughness, metallographic structure, and work hardening, in orthogonal turn-milling. This study provides strong

guidance for exploring the machinability of difficult-to-cut materials in orthogonal turn-milling and helps improve the applicability of orthogonal turn-milling to difficult-to-cut materials.

2 Experimental setup and procedures

2.1 Workpiece

The experimental material is TC21, and the diameter of the experimental bar is 100 mm. As shown in Fig. 1, TC21 has an initial basket-weave microstructure. The chemical compositions of TC21 are given in Table 1 [6].

Table 1 Chemical compositions of TC21 [6]

| Composition | Weight percent/wt.% |
|-------------|---------------------|
| Al | 6.78 |
| Mo | 2.87 |
| Sn | 2.32 |
| Nb | 2.31 |
| Zr | 2.19 |
| Cr | 0.77 |
| Si | 0.09 |
| Ti | Balance |

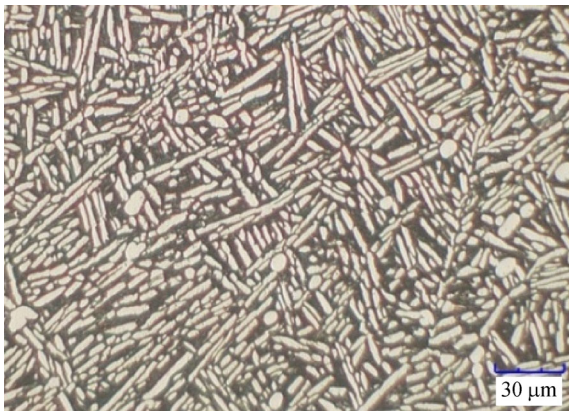


Fig. 1 Microstructure of raw TC21.

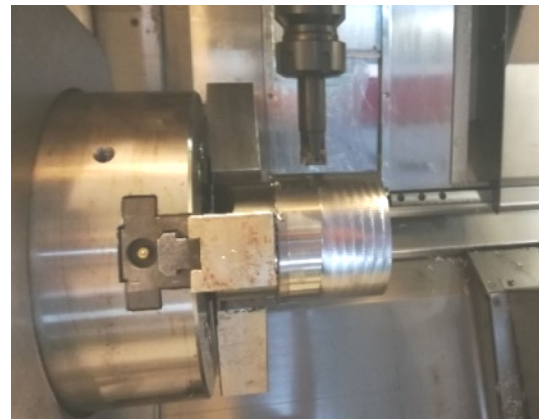


Fig. 2 Photograph of cutting via turn-milling.

2.2 Test equipment

The experimental machine tool is a Mazak Integrex 200-IVST. The main parameters of the machine tool are as follows: Maximum rotary tool spindle speed of 1200 r/min, rated power of 25 kW, and maximum feed speed of 38 m/min. The experiment status is shown in Fig. 2.

The experimental cutting tool includes a tool holder and

an insert, as shown in Fig. 3. For the insert, the specification is ISO standard R390-11 T3 08E-PLW 1130 (Sandvik), the rake and clearance angles are 16° and 12°, respectively, and the outer coating is TiAlN. For the tool holder, the specification is ISO standard R390-020A22-11M, and the cutting diameter is 20 mm.

In orthogonal turn-milling, the cutting process of the bottom flank face of the tool forms the machined surface of the workpiece. Therefore, the wear of the bottom flank face

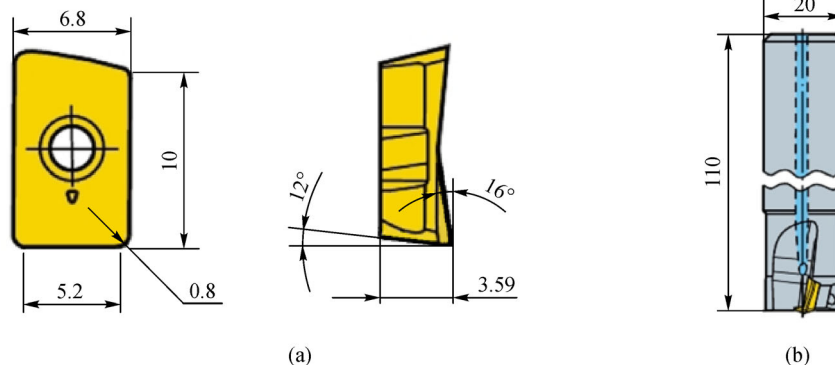


Fig. 3 Dimensions of the insert and tool holder for turn-milling. (a) R390-11 T3 08E-PLW 1130 insert and (b) R390-020A22-11M tool holder. Unit: mm.

of the insert is used to determine whether the tool has failed or not. Tool failure corresponds to a wear value exceeding 0.2 mm for regular tool wear or 0.4 mm for irregular tool wear.

The flank wear value of the insert and the metallographic microstructure of the machined surface are measured with a KH-7700 digital microscope. Tool failure is measured using a Hitachi S-3400 scanning electron microscope (SEM) capable of energy-dispersive X-ray spectroscopy (EDS). The microhardness of the machined surface is measured using an HXS-1000A digital microhardness tester, and the surface roughness is measured with a Mahr M1 portable roughness meter.

2.3 Cutting parameters

As shown in Fig. 4, orthogonal turn-milling involves three movements, namely, workpiece rotation, axial movement, and tool rotation. Based on the direction and distance of the workpiece and tool axes and the direction of y_w in Fig. 5, the eccentricity in orthogonal turn-milling can be zero, positive, or negative.

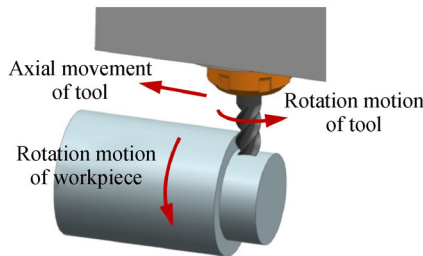


Fig. 4 Three movements in orthogonal turn-milling.

As shown in Fig. 5 and Table 2, orthogonal turn-milling involves more cutting parameters than turning does; l_t is

the blade width of the tool, Z is the tooth number, r_w is the workpiece radius, and the other parameters are given in Table 2.

3 Results and discussion

3.1 Failure of TiAlN-coated tool in orthogonal turn-milling of titanium alloy TC21

3.1.1 Tool life

For the orthogonal turn-milling of TC21, Fig. 6 shows how tool life depends on the cutting parameters. Given that the wear of the bottom flank face of the tool is irregular, a wear value greater than 0.4 mm is considered tool failure, and the corresponding time is the tool life.

A comparison of tool life in down milling and up milling is shown in Fig. 6(a). Down milling has a longer tool life than up milling. The cutting thickness increases gradually during the orthogonal turn-milling of TC21 in up milling. Thus, the extrusion and friction between the cutting edge and workpiece are aggravated when the cutting edge enters the workpiece, and the titanium can easily stick on the cutting edge. The impact of the cutting edge with the adhesive titanium accelerates the tool wear because turn-milling involves interrupted cutting. Hence, we recommend down milling in orthogonal turn-milling.

Cutting force affects tool wear and can therefore be used to evaluate the cause of changes in tool life. Cutting force cannot be measured with a general dynamometer because the tool rotates together with the workpiece in orthogonal turn-milling. To solve this problem, the chip volume is used to evaluate tool life because the former is proportional to cutting force. An electronic scale with a precision of 0.01 g is utilized to measure the chip weight, and chip volume V is calculated indirectly by using the material

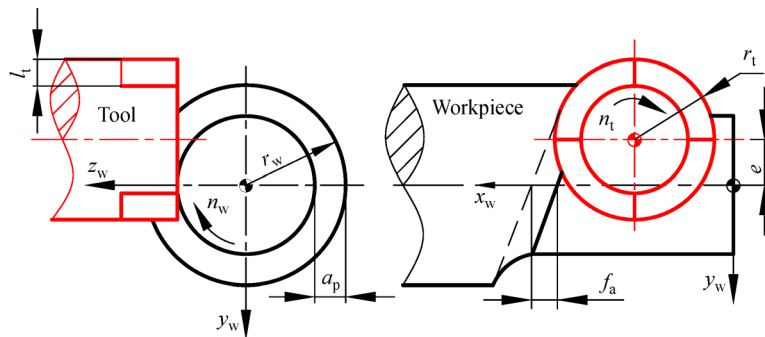


Fig. 5 Eccentricity of orthogonal turn-milling.

Table 2 Cutting parameters in the orthogonal turn-milling experiments

| Tool speed $n_t/(r \cdot \text{min}^{-1})$ | Workpiece speed $n_w/(r \cdot \text{min}^{-1})$ | Cutting depth a_p/mm | Feed rate per revolution $f_a/(\text{mm} \cdot r^{-1})$ | Eccentricity e/mm |
|--|---|-------------------------------|---|----------------------------|
| 1500, 2000, 2500 | 2, 5, 8 | 0.5, 1, 1.5 | 2, 4, 6 | -8, 0, 8 |

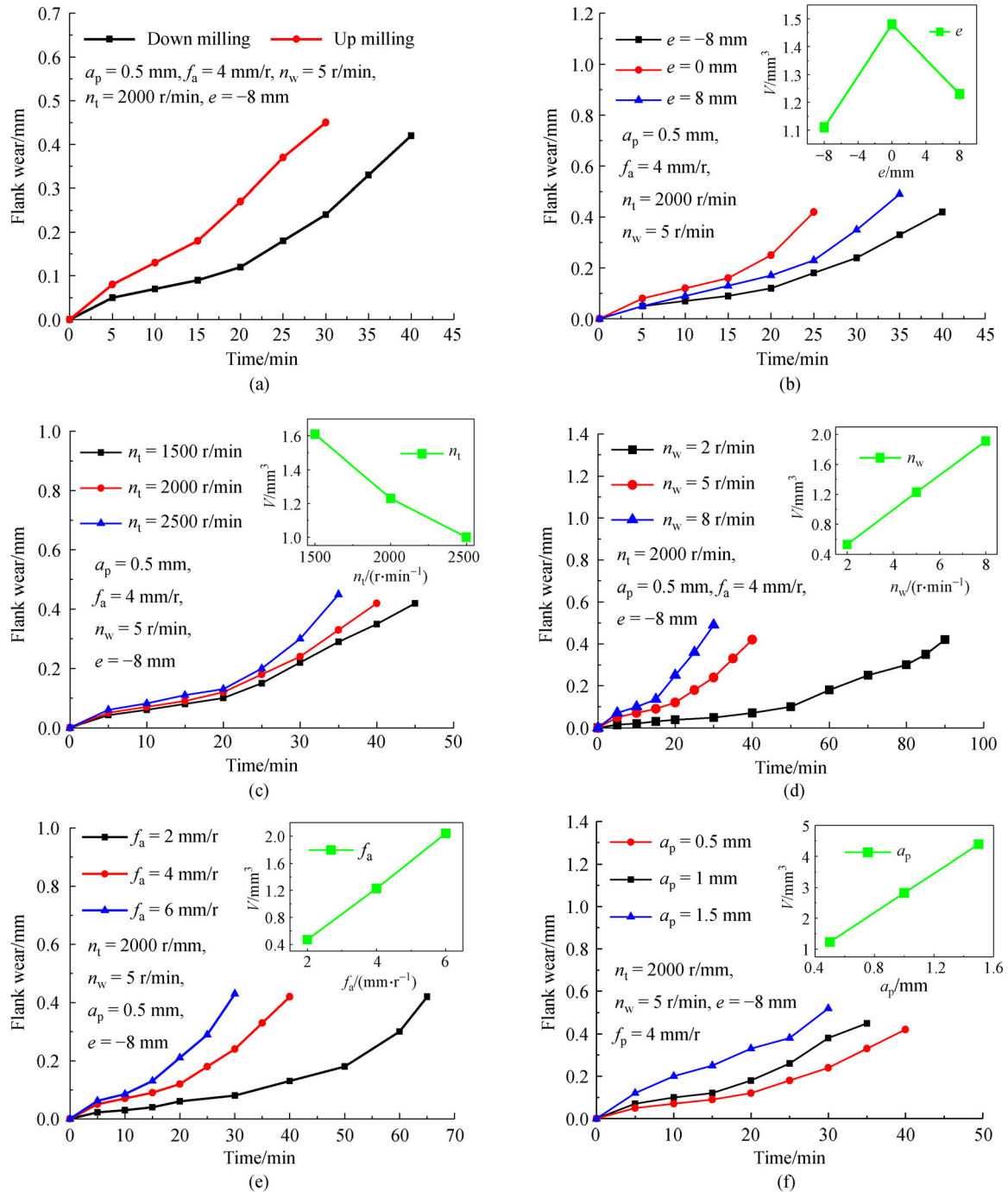


Fig. 6 Effects of parameters on tool life in orthogonal turn-milling: (a) Down milling and up milling, (b) eccentricity e , (c) tool speed n_t , (d) workpiece speed n_w , (e) feed rate per revolution f_a , and (f) cutting depth a_p .

density of the workpiece in orthogonal turn-milling. The measured results are shown in the upper-right corner of Fig. 6.

As presented in Fig. 6(b), tool life is longer with a positive or negative eccentricity e than it is with non-eccentric orthogonal turn-milling ($e = 0$). Chip volume V is 1.11, 1.48, and 1.23 mm³ for $e = -8$, 0, and 8 mm, respectively. A large chip volume causes a large cutting

force in the same cutting time, so the cutting force is the maximum for $e = 0$. A large cutting force aggravates the tool wear process, thereby shortening the tool life. By contrast, a large eccentricity means that the bottom of the cutting edge has a large contact area with the workpiece; this reduces the pressure on the tool surface and lengthens the tool life. The tool life is the longest (i.e., 41 min) for $e = -8$ mm. Hence, we use $e = -8$ mm in our subsequent

orthogonal turn-milling experiments.

As shown in Fig. 6(c), with $a_p = 0.5$ mm, $f_a = 4$ mm/r, $n_w = 5$ r/min, and $e = -8$ mm, the tool life is 43 and 33 min under $n_t = 1500$ and 2500 r/min, respectively. When tool speed n_t is increased, the reducing chip volume decreases the cutting force. In addition, increasing n_t reduces the time between the tool entering and leaving the workpiece, thereby making the cutting process smooth and decreasing the mechanical impact. These aspects help reduce tool wear. However, increasing n_t also increases the cutting heat, which aggravates tool wear. Consequently, the above combination of effects means that tool life does not decrease considerably when n_t is increased.

As shown in Fig. 6(d), with $a_p = 0.5$ mm, $f_a = 4$ mm/r, $n_t = 2000$ r/min, and $e = -8$ mm, the tool life is 89 and 27 min under $n_w = 2$ and 8 r/min, respectively. The chip volume increases with increasing n_w , and the cutting force, mechanical impact, and temperature increase with increasing n_w . Hence, the tool life decreases.

As shown in Fig. 6(e), the tool life is 65 and 29 min at a feed rate per revolution of $f_a = 2$ and 6 mm/r, respectively. The tool life decreases with f_a for the same reasons that it does so with n_w .

As shown in Fig. 6(f), the tool life is 39 and 26 min under $a_p = 0.5$ and 1.5 mm, respectively. The tool life decreases with a_p for the same reasons that it does so with n_w .

We experimentally explore the longer tool life under orthogonal turn-milling than under turning, and the results are shown in Fig. 7. We use three tool teeth with TiAlN coating in orthogonal turn-milling for down milling, with $n_t = 2000$ r/min, $n_w = 5$ r/min, $f_a = 4$ mm/r, $e = -8$ mm, and $a_p = 1$ mm. The wear process of each tooth is different; hence, to measure the tool life of orthogonal turn-milling, we use the tooth of first to tool failure criteria. The corresponding tool life is 79 min, and the MRR is 5 cm³/min.

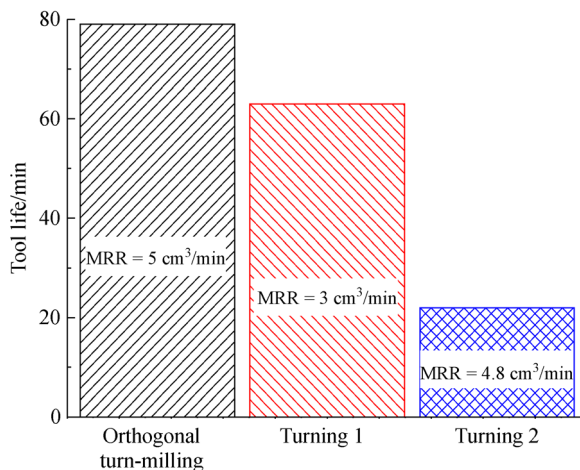


Fig. 7 Tool life and material removal rate of turning and orthogonal turn-milling for TC21.

We use the same coated tool for orthogonal turn-milling and turning. The cutting parameters for the first turning experiment are cutting speed $v = 100$ m/min, $a_p = 0.6$ mm, and feed rate $f = 0.05$ mm/r; the corresponding tool life is 63 min, and MRR is 3 cm³/min. The cutting parameters for the second turning experiment are $v = 80$ m/min, $a_p = 0.6$ mm, and $f = 0.1$ mm/r; the corresponding tool life is 22 min, and MRR is 4.8 cm³/min. Orthogonal turn-milling helps reduce the cutting force and temperature compared with turning [19], so the tool life in orthogonal turn-milling is higher than that in turning when cutting TC21 for a high MRR.

3.1.2 Tool failure process

By experimenting with orthogonal turn-milling, we obtain the following findings. During the initial stage of tool wear, the wear of the flank face is even, no chipping or coating shedding is observed in this area, and minimal chipping and coating shedding occur on the rake face of the insert, as shown in Fig. 8(a). As the cutting process develops, large chips appear at the round corner of the rake face, the tool wear at the round corner is enlarged, and the wear of the entire cutting edge becomes uneven for the flank face, as shown in Fig. 8(b). During the stage of rapid wear, the cutting force and impact increase rapidly because the wear and chipping of the insert's round corner increase. The continuous mechanical impact on the round corner of the rake face leads to fragmentation, which influences the flank face and leads to further fragmentation at the round corner of the flank face. Then, the chipping of the insert corner transforms into large fragmentation in a very short time, as shown in Fig. 8(c).

In the orthogonal turn-milling cutting process, we can assume that the workpiece is at rest and that the tool moves spirally along the axis of the workpiece. As shown in Fig. 9, when the tool moves from position 1 to position 2, the intersected portion of the two tool positions and the workpiece can be viewed as the geometrical shape of the cutting layer in orthogonal turn-milling. On the basis of this geometrical shape, the side and bottom cutting edges participate simultaneously in the cutting, and the stress is concentrated on the round corner of the insert; hence, tool failure (e.g., fragmentation) easily occurs there.

3.1.3 Tool failure mechanism

To investigate the mechanism of tool failure in the orthogonal turn-milling of TC21, the round corner of the flank face is observed using SEM during the failure stage of the insert. As shown in Fig. 10, several cracks are parallel to the cutting edge, but no cracks are perpendicular to the cutting edge. The cemented carbide of the base material appears after tool failure. The cracks parallel to the cutting edge are caused by mechanical impact, whereas

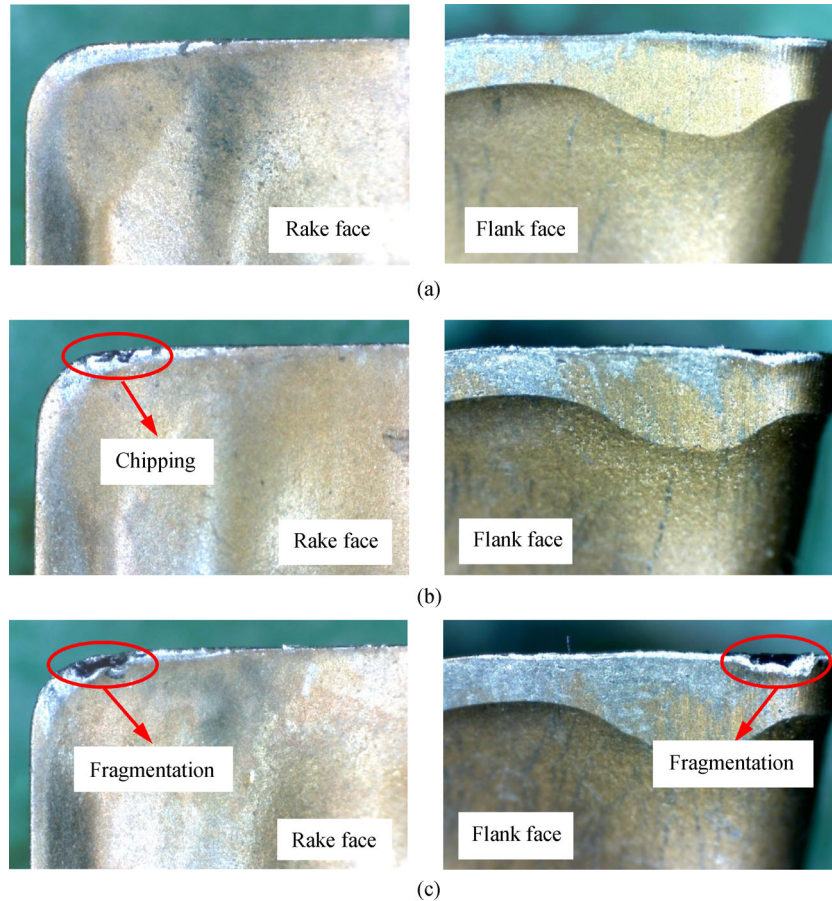


Fig. 8 Failure process of the insert in orthogonal turn-milling ($n_t = 2000$ r/min, $n_w = 5$ r/min, $f_a = 4$ mm/r, $e = -8$ mm, $a_p = 0.5$ mm). (a) Cutting time = 17 min, flank-face wear of insert = 0.1 mm (20 \times); (b) cutting time = 24 min, flank-face wear of insert = 0.17 mm (20 \times); (c) cutting time = 32 min, flank-face wear of insert = 0.28 mm (20 \times).

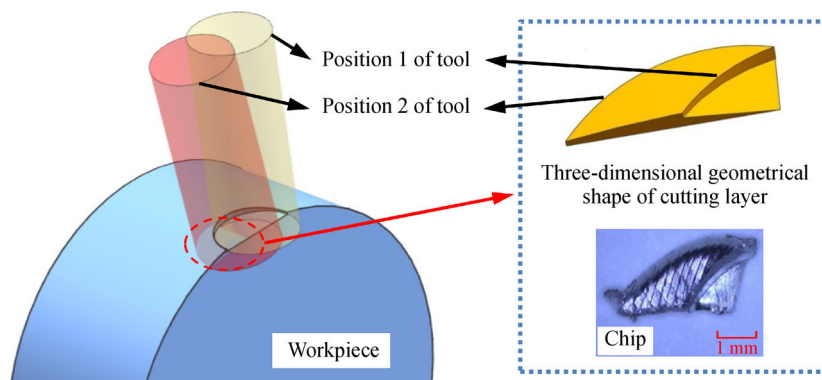


Fig. 9 Formation of the cutting layer in orthogonal turn-milling.

any cracks perpendicular to the cutting edge would be heat cracks caused by a high cutting temperature. The absence of the latter in the present case shows that the cutting temperature is low in orthogonal turn-milling, and the heat shock that causes heat cracks is avoided.

According to Fig. 8 and the correlative analyses, the

degree of failure at the rake face is higher than that at the flank face. Consequently, the round corner of the rake face is observed using SEM during the failure stage of the insert, as shown in Fig. 11. As the fragmentation of the round corner on the insert grows, the insert becomes increasingly blunt, and the cutting force and temperature

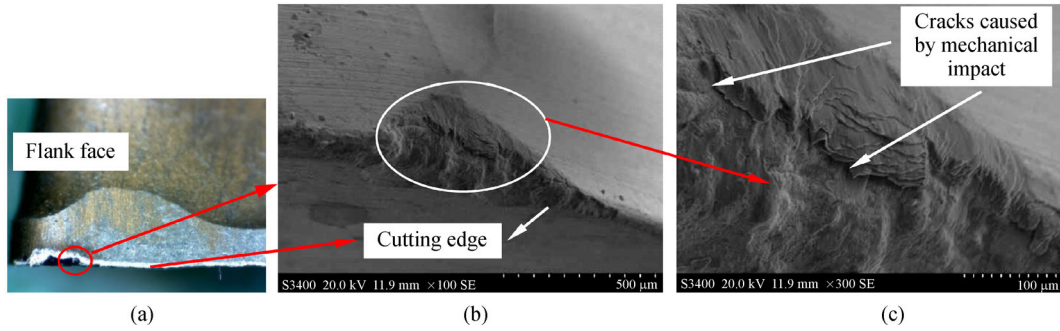


Fig. 10 Scanning electron microscope (SEM) images of the round corner of the flank face in the failure stage of the insert. (a) Failed tool; SEM image magnified (b) 100 \times and (c) 300 \times .

increase rapidly. Under high temperature and pressure, the Ti alloy adheres easily to the tool mainly because the former has lower hardness, higher chemical reactivity, and stronger affinity than the latter. In the cutting process of orthogonal turn-milling, the chips flow over the rake face of the insert, thus generating high temperature and pressure. Consequently, the degree of adhesive wear on the rake face is higher than that on the flank face. When adhesion occurs, stripping also does because of the adhesive layer, thereby causing the adhesion wear that is responsible for the failure of the cutting tool. Figure 11 shows the existence of some adhesive material and stripping on the rake face, indicating the presence of serious adhesive wear on the rake face of the insert in the tool failure stage.

To explore the orthogonal turn-milling tool failure mechanism further, we perform EDS at two points in Fig. 11: Point 1 corresponds to the adhered Ti, and point 2 corresponds to a stripping location. The chemical compositions of the points are shown in Fig. 12 and given in Table 3.

The EDS results show that point 1 corresponds to the adhered Ti because its composition contains a large amount of Ti. In the failure stage of the insert, the cemented carbide of the base material has already appeared

at point 1. The main elements of cemented carbide are C, W, and Co, and those of TC21 are Ti, Al, Mo, and Sn (Table 1). The Ti content of point 1 far exceeds that of cemented carbide, thereby verifying the existence of serious adhesive wear in orthogonal turn-milling.

Figure 12 and Table 3 show that the tool surface contains C and Ti atoms. The intermittent cutting process of orthogonal turn-milling causes a high cutting temperature gradient at the cutting edge. With the high cutting temperature gradient, the Ti atoms in the workpiece material diffuse rapidly to the tool coating, where they combine with C atoms of the tool coating material to form a TiC layer. The combined effect of mechanical force and impact strips this TiC layer from the tool surface, thereby generating fresh diffusive wear [25]. However, because the content of C atoms in the TiAlN tool coating is relatively low, this diffusive wear has little influence on tool wear.

The presence of O atoms in Fig. 12 and Table 3 indicates the existence of oxidation on the rake face of the insert. The Al atoms of the insert spread outward and combine with atmospheric O atoms to form a dense outer layer of Al₂O₃. This shield prevents O atoms from spreading inward into the coating, thus improving the antioxidant properties of the tool coating. Meanwhile, the Ti atoms of the tool coating spread inward and combine with

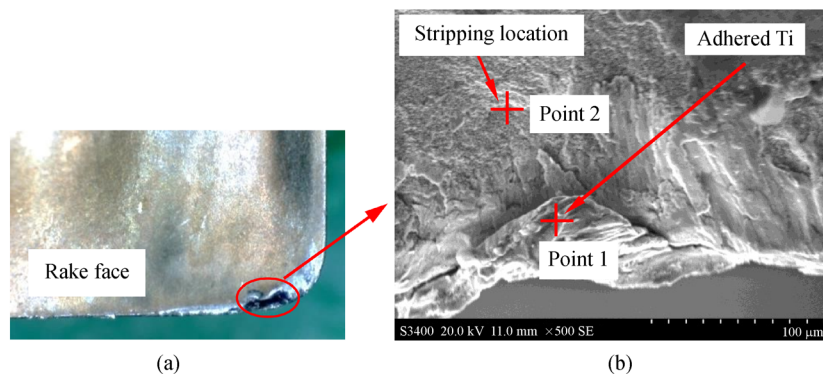


Fig. 11 Scanning electron microscope (SEM) image of the round corner of the rake face in the failure stage of the insert. (a) Failed tool and (b) SEM image magnified 500 \times .

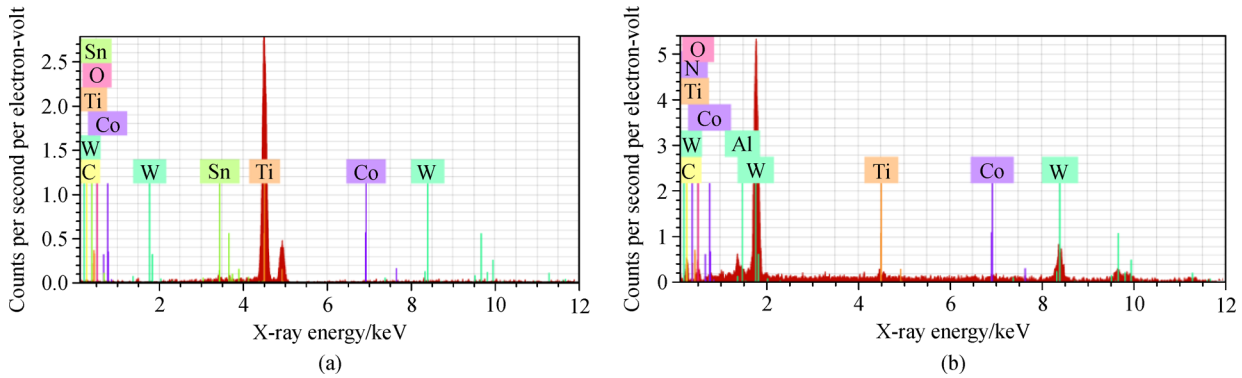


Fig. 12 Energy-dispersive X-ray spectroscopy of points 1 and 2 in Fig. 11. (a) Point 1 and (b) point 2.

Table 3 Chemical compositions of points 1 and 2

| Point | Chemical composition/wt.% | | | | | | | |
|---------|---------------------------|------|------|-------|-------|------|------|------|
| | Ti | O | Sn | W | C | Co | N | Al |
| Point 1 | 93.28 | 2.45 | 1.67 | 1.43 | 1.04 | 0.13 | 0.00 | 0.00 |
| Point 2 | 1.02 | 7.89 | 0.00 | 71.44 | 16.41 | 2.08 | 0.77 | 0.40 |

atmospheric O atoms to form an inner TiO_2 layer [25]. At high cutting temperatures, the linear expansion coefficients of this oxidation layer and the tool base material differ, which causes heat stress and cracking and stripping of the tool coating.

The cutting force and temperature increase as the tool wear increases, and this increased stress and temperature lead to serious adhesive wear between the tool and workpiece. Under the influence of drastic mechanical impact, the adhesive material is stripped, and the EDS performed at a stripping location (point 2) shows many C, W, and Co atoms and few Ti ones. This result indicates that the cemented carbide of the tool base material appears at this location after adhesion and stripping, and high stress and temperature cause serious diffusion and oxidation wear that aggravate the progress of tool wear.

3.2 Machined surface integrity in orthogonal turn-milling of titanium alloy TC21

3.2.1 Analysis of surface roughness

The machined surface roughness, R_a , in the axial direction obtained for a workpiece using different cutting parameters is shown in Fig. 13. Eccentricity e has a significant influence on tool life. With increasing e , the bottom of the cutting edge has a large contact area with the workpiece, thus reducing the cutting force and cutting vibrations. This condition leads to improved machining stability and reduced R_a (Fig. 13(a)).

For $n_t = 2000$ r/min, an increasing n_w means that the ratio $\lambda = n_t/n_w$ decreases, and the chip volume increases.

This condition causes the machined surface profile to be rugged, thereby increasing R_a . Moreover, the high chip volume increases the cutting force and vibrations and worsens R_a . In conclusion, λ has a significant influence on R_a (Fig. 13(b)).

The effect of f_a on R_a is shown in Fig. 13(c). We have $R_a = 0.25$ and 0.30 μm for $f_a = 2$ and 6 mm/r, respectively, which indicates that the effect of f_a on R_a is not significant. MRR increases with f_a , leading to an increase in cutting force and R_a .

3.2.2 Analysis of the metallographic structure

The specimens are machined via wire electrical discharge machining, and the mirror effect of the cross section of the specimens is obtained sequentially through rough grinding, precision grinding, and polishing. The polished surfaces are treated with a corrosive liquid (2% HF + 4% HNO_3 + 94% H_2O) for 15 s. Then, the metallographic microstructure of the specimens is measured.

As shown in Fig. 14, we use cutting parameters that correspond to either a short or long tool life (T) to obtain clear views of the metallographic structure of the machined surface layer. As shown in Figs. 14(a) and 14(b), with a short T , no obvious grain deformation (e.g., stretches, recrystallization, and tears) is observed. The same applies to the case of a long T , as shown in Figs. 14(c) and 14(d). Orthogonal turn-milling involves interrupted cutting and high-speed machining, which result in reduced cutting temperature and force; thus, grain deformations do not form easily in the metallographic structure of the surface layer.

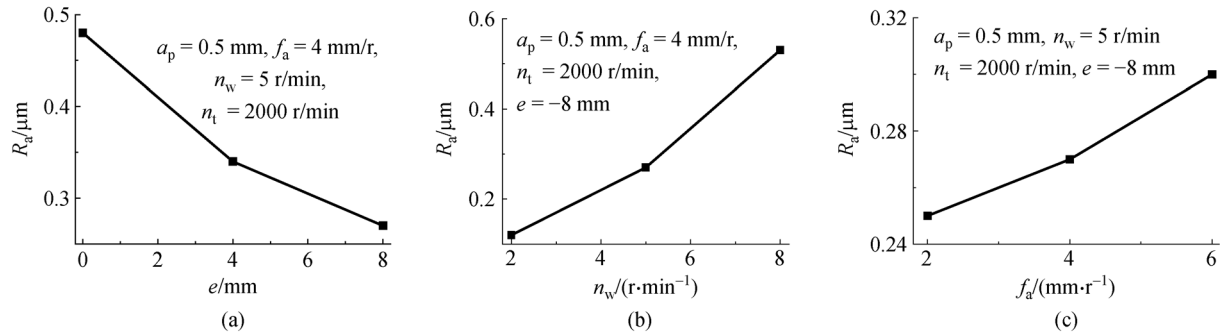


Fig. 13 Effects of (a) eccentricity e , (b) workpiece speed n_w , and (c) feed rate per revolution f_a on R_a in orthogonal turn-milling.

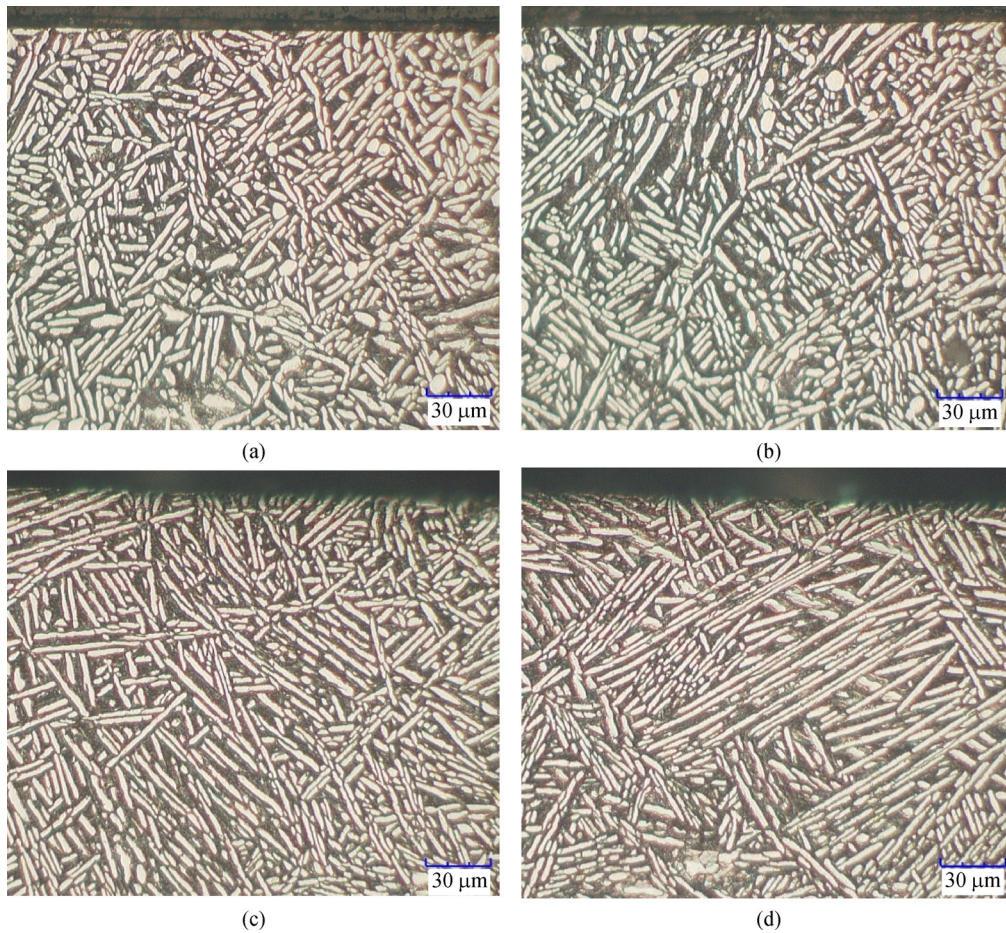


Fig. 14 Metallographic structure of the machined surface layer in orthogonal turn-milling. (a) $a_p = 0.5$ mm, $n_t = 2000$ r/min, $n_w = 8$ r/min, $e = -8$ mm, $f_a = 4$ mm/r, $Z = 1$, and $T = 27$ min; (b) $a_p = 0.5$ mm, $n_t = 2500$ r/min, $n_w = 5$ r/min, $e = -8$ mm, $f_a = 4$ mm/r, $Z = 1$, and $T = 33$ min; (c) $a_p = 0.5$ mm, $n_t = 2000$ r/min, $n_w = 2$ r/min, $e = -8$ mm, $f_a = 4$ mm/r, $Z = 1$, and $T = 88$ min; (d) $a_p = 0.5$ mm, $n_t = 2000$ r/min, $n_w = 5$ r/min, $e = -8$ mm, $f_a = 2$ mm/r, $Z = 1$, and $T = 64$ min.

3.2.3 Analysis of work hardening

As presented in Fig. 15, we use the cutting parameters from Fig. 14 to check the microhardness of the machined surface layer. The matrix microhardness of the raw TC21 alloy in this experiment is in the range of 340 to 370 HV. The experiments show that the microhardness of the machined

surface layer is also in this range. No obvious work hardening is observed when using cutting parameters that provide either a long or short tool life. In cutting with orthogonal turn-milling, the cutting temperature is low, which reduces the softening of the surface layer of the workpiece. Moreover, the cutting force is low, so the grains are unlikely to be deformed. For these reasons, no work

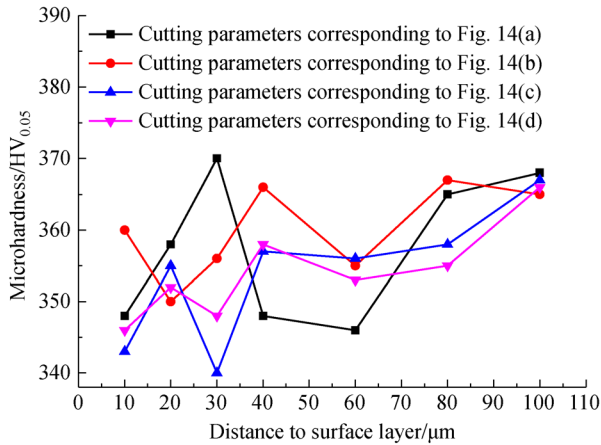


Fig. 15 Microhardness of the machined surface layer in orthogonal turn-milling.

hardening of the surface layer is observed, which is in accordance with our analysis of the metallographic structure.

On the basis of these discussions and the use of a tool coated with TiAlN (one tooth) to cut a 100-mm-diameter bar of TC21 alloy, our research shows that orthogonal turn-milling is suitable for down milling and negative eccentricity. For $e = -8$ mm, we recommend the following orthogonal turn-milling parameters: (i) Tool speed $n_t = 1500$ to 2000 r/min, (ii) workpiece speed $n_w = 2$ to 5 r/min, (iii) feed rate per revolution $f_a = 2$ to 4 mm/r, and (iv) cutting depth $a_p = 0.5$ to 1 mm. The corresponding tool life is 40 to 91 min, the MRR is 0.5 to 5 cm³/min, the surface roughness is 0.12 to 0.53 μm, and no obvious grain deformation and work hardening are observed.

4 Conclusions

With regard to increasing the tool life in orthogonal turn-milling, down milling is better than up milling, and negative eccentricity is better than either zero or positive eccentricity. Tool life decreases when any of the cutting parameters (n_t , a_p , n_w , and f_a) are increased. To improve the machined surface integrity, we should use a large e and a small n_w . These parameters exert more influence than f_a does on the machined surface roughness. To reduce surface roughness, we should increase n_t . Moreover, to increase machining efficiency, we should increase a_p and f_a . No obvious grain deformation or work hardening is observed in the experiments.

When using a TiAlN-coated tool to cut TC21 via orthogonal turn-milling, tool failure is characterized by the following: (i) Large fragmentation, (ii) the degree of failure of the rake face is higher than that of the flank face, and (iii) tool failure is generated easily on the round corner of the tool. Adhesive wear plays a vital role as the wear mechanism of the TiAlN-coated tool for cutting TC21

via orthogonal turn-milling. Under mechanical impact action, the combination of adhesive wear, diffusive wear, and oxidation leads to increasingly serious tool damage, which results in tool failure.

With the MRR of orthogonal turn-milling being higher than that of turning, the tool life of orthogonal turn-milling is higher than that of turning when cutting TC21. When using a tool coated with TiAlN (one tooth) to cut a 100-mm-diameter bar of TC21 alloy with $e = -8$ mm, the following orthogonal turn-milling parameters are recommended: (i) Tool speed $n_t = 1500$ to 2000 r/min, (ii) workpiece speed $n_w = 2$ to 5 r/min, (iii) feed rate per revolution $f_a = 2$ to 4 mm/r, and (iv) cutting depth $a_p = 0.5$ to 1 mm.

Acknowledgements The authors gratefully acknowledge the financial support provided by the Natural Science Foundation of Jiangsu Province (Grant No. BK20171170), the Six Talent Peaks Project of Jiangsu Province (Grant No. JXQC-049), the Major Program of Natural Science Foundation for Colleges and Universities of Jiangsu Province (Grant No. 19KJA560007), and the Project of Jiangsu Key Laboratory of Large Engineering Equipment Detection and Control (Grant No. JSKLEDC201512).

References

- Sun T, Fu Y C, He L, et al. Machinability of plunge milling for damage-tolerant titanium alloy TC21. *International Journal of Advanced Manufacturing Technology*, 2016, 85(5–8): 1315–1323
- Wang P, Nai M L S, Sin W J, et al. Effect of overlap distance on the microstructure and mechanical properties of *in situ* welded parts built by electron beam melting process. *Journal of Alloys and Compounds*, 2019, 772: 247–255
- Wang P, Todai M, Nakano T. Beta titanium single crystal with bone-like elastic modulus and large crystallographic elastic anisotropy. *Journal of Alloys and Compounds*, 2019, 782: 667–671
- Shi Q, Li L, He N, et al. Experimental study in high speed milling of titanium alloy TC21. *International Journal of Advanced Manufacturing Technology*, 2013, 64(1–4): 49–54
- Shi Q, He N, Li L, et al. Analysis on surface integrity during high speed milling for new damage-tolerant titanium alloy. *Transactions of Nanjing University of Aeronautics & Astronautics*, 2012, 29(3): 222–226
- Sun T, Fu Y C, He L, et al. Cutting machinability for damage-tolerant titanium alloy. *Journal of Shanghai Jiaotong University*, 2016, 50(7): 1017–1022 (in Chinese)
- Zhang H X, Zhao J, Wang F Z, et al. Cutting forces and tool failure in high-speed milling of titanium alloy TC21 with coated carbide tools. *Proceedings of the Institution of Mechanical Engineers, Part B: Journal of Engineering Manufacture*, 2015, 229(1): 20–27
- Wang P, Wu L, Feng Y, et al. Microstructure and mechanical properties of a newly developed low Young's modulus Ti–15Zr–5Cr–2Al biomedical alloy. *Materials Science and Engineering: C*, 2017, 72: 536–542
- Schulz H, Spur G. High speed turn-milling—A new precision manufacturing technology for the machining of rotationally

- symmetrical workpieces. *CIRP Annals*, 1990, 39(1): 107–109
10. Schulz H, Kneisel T. Turn-milling of hardened steel—An alternative to turning. *CIRP Annals*, 1994, 43(1): 93–96
 11. Choudhury S K, Mangrulkar K S. Investigation of orthogonal turn-milling for the machining of rotationally symmetrical work pieces. *Journal of Materials Processing Technology*, 2000, 99(1–3): 120–128
 12. Choudhury S K, Bajpai J B. Investigation in orthogonal turn-milling towards better surface finish. *Journal of Materials Processing Technology*, 2005, 170(3): 487–493
 13. Ekinović S, Begović E, Silajdžija A. Comparison of machined surface quality obtained by high-speed machining and conventional turning. *Machining Science and Technology*, 2007, 11(4): 531–551
 14. Pogacnik M, Kopac J. Dynamic stabilization of the turn-milling process by parameter optimization. *Proceedings of the Institution of Mechanical Engineers. Part B: Journal of Engineering Manufacture*, 2000, 214(2): 127–135
 15. Zhu L D, Li H N, Wang W S. Research on rotary surface topography by orthogonal turn-milling. *International Journal of Advanced Manufacturing Technology*, 2013, 69(9–12): 2279–2292
 16. Ratnam C, Arun Vikram K, Ben B S, et al. Process monitoring and effects of process parameters on responses in turn-milling operations based on SN ratio and ANOVA. *Measurement*, 2016, 94: 221–232
 17. Karagüzel U, Bakkal M, Budak E. Process modeling of turn-milling using analytical approach. *Procedia CIRP*, 2012, 4: 131–139
 18. Uysal E, Karagüzel U, Budak E, et al. Investigating eccentricity effects in turn-milling operations. *Procedia CIRP*, 2014, 14: 176–181
 19. Karagüzel U, Uysal E, Budak E, et al. Analytical modeling of turn-milling process geometry, kinematics and mechanics. *International Journal of Machine Tools and Manufacture*, 2015, 91: 24–33
 20. Karaguzel U, Bakkal M, Budak E. Mechanical and thermal modeling of orthogonal turn-milling operation. *Procedia CIRP*, 2017, 58: 287–292
 21. Niu Z K, Jiao L, Chen S Q, et al. Surface quality evaluation in orthogonal turn-milling based on box-counting method for image fractal dimension estimation. *Nanomanufacturing and Metrology*, 2018, 1(2): 125–130
 22. Berenji K R, Kara M E, Budak E. Investigating high productivity conditions for turn-milling in comparison. *Procedia CIRP*, 2018, 77: 259–262
 23. Benjamin C, Andreas N, Andreas C, et al. Investigation of surface properties in turn milling of particle-reinforced aluminium matrix composites using MCD-tipped tools. *International Journal of Advanced Manufacturing Technology*, 2019, 8: 1–14
 24. Sun T, Qin L F, Fu Y C, et al. Chatter stability of orthogonal turn-milling analyzed by complete discretization method. *Precision Engineering*, 2019, 56: 87–95
 25. An Q, Chen J, Tao Z, et al. Experimental investigation on tool wear characteristics of PVD and CVD coatings during face milling of Ti6242S and Ti-555 titanium alloys. *International Journal of Refractory Metals & Hard Materials*, 2020, 86: 105091